

# Journal of Materials Chemistry A

Accepted Manuscript



This is an *Accepted Manuscript*, which has been through the Royal Society of Chemistry peer review process and has been accepted for publication.

*Accepted Manuscripts* are published online shortly after acceptance, before technical editing, formatting and proof reading. Using this free service, authors can make their results available to the community, in citable form, before we publish the edited article. We will replace this *Accepted Manuscript* with the edited and formatted *Advance Article* as soon as it is available.

You can find more information about *Accepted Manuscripts* in the [Information for Authors](#).

Please note that technical editing may introduce minor changes to the text and/or graphics, which may alter content. The journal's standard [Terms & Conditions](#) and the [Ethical guidelines](#) still apply. In no event shall the Royal Society of Chemistry be held responsible for any errors or omissions in this *Accepted Manuscript* or any consequences arising from the use of any information it contains.

## REVIEW

**Harnessing single-active plasmonic nanostructures for enhanced photocatalysis under visible light**

Cite this: DOI: 10.1039/x0xx00000x

Hefeng Cheng,<sup>a</sup> Kojiro Fuku,<sup>a</sup> Yasutaka Kuwahara,<sup>ab</sup> Kohsuke Mori<sup>ab</sup> and Hiromi Yamashita<sup>\*ab</sup>Received 00th January 2012,  
Accepted 00th January 2012

DOI: 10.1039/x0xx00000x

www.rsc.org/

The past several decades have witnessed the fast-growing field of plasmonics that localize and concentrate the incident light at the nanoscale, providing the source of light, heat and energetic carriers. Plasmonic nanostructures, which are able to harvest and convert the abundant sunlight to drive chemical reactions, have shown great prospects in heterogeneous photocatalysis. To maximize solar energy utilization, rational design and precise manipulation of the plasmonic nanostructures are therefore essential for their strong light-matter interaction. In this review, we focus on the very recent advances in harnessing single-active plasmonic nanocatalysts (that is, plasmonic materials as the only photo- and catalytic-active species), involving noble metals and doped-semiconductors, for enhanced photocatalytic reactions with visible light.

**1. Introduction**

Heterogeneous catalysis, which employs catalysts to drive or facilitate the chemical reactions, is of paramount importance to chemical and energy industries. To activate the reaction, in most cases higher temperature is required to conquer the potential barrier, leading to huge energy consumption. As an alternative to traditional fossil fuels, solar energy is by far the largest detectable resource to fulfil the increasing worldwide energy demands for its great abundance, environmentally benign nature and in particular the renewable availability.<sup>1</sup> Through introduction of light irradiation, it will alter the thermodynamical equilibrium and may enable the chemical reactions to be implemented at ambient conditions instead of the thermal treatments.<sup>2</sup> Sunlight-driven catalytic reactions could be actualized via either semiconductor photocatalysis,<sup>3–7</sup> where photo-generated electrons/holes upon light excitation would participate in the subsequent reduction/oxidation processes, or by the plasmon-mediated photocatalysis.<sup>8</sup>

Since the discovery of Honda-Fujishima effect on the TiO<sub>2</sub> photoelectrode,<sup>3</sup> semiconductor photocatalysis has played a great role in energy exploitation and environmental decontamination, which allows water reduction into H<sub>2</sub> or toxic

pollutant molecules oxidation.<sup>4–7</sup> Nevertheless, the intrinsic wide band gaps (WBG, >3.1 eV) render the conventional used semiconductors (*e.g.*, TiO<sub>2</sub>, ZnO) solely responsive to ultraviolet (UV) light. Furthermore, under UV irradiation, the involvement of active oxygen radical intermediates such as superoxide anion radical (O<sub>2</sub><sup>•-</sup>) and hydroxyl radical (•OH) is usually non-selective, thereby resulting in the complete decomposition of organic molecules into small inorganic species (CO<sub>2</sub>, H<sub>2</sub>O, etc.).<sup>7</sup> In terms of energy proportion, sunlight contains less than 5% of UV light, while visible light (400–800 nm) accounts for the majority (*ca.* 43%). Therefore, it is more appealing to develop visible light driven photocatalysis with narrow band gap (NBG) semiconductors, which entail broader visible light absorption and higher selectivity towards organic synthesis.

Nanostructured plasmonic metals such as Au, Ag and Cu represent another class of important materials that strongly absorb visible light in a wide range of the solar spectrum owing to their localized surface plasmon resonance (LSPR).<sup>8–11</sup> LSPR can be described as the collective oscillation of free conduction electrons confined in metallic nanoparticles (NPs) resonant with the incident light. As a consequence, light is amplified in the near-field region of plasmonic NPs, and it has led to an array of applications in as diverse as surface-enhanced Raman

spectroscopy (SERS),<sup>12–14</sup> single-molecule spectroscopy,<sup>15,16</sup> solar cells<sup>17</sup> and biological molecular detection/sensing.<sup>18</sup> Recently, plasmonic metal NPs have been used to sensitize semiconductors and boost their photocatalytic performances by construction of the noble metal/semiconductor hybrids under visible light.<sup>19–26</sup> Arising from the LSPR effect, plasmonic NPs are able to transfer solar energy to the neighboring semiconductors<sup>19–26</sup> or molecular complexes<sup>27</sup> to drive chemical reactions. Intriguingly, in addition to performing as the visible light absorber, plasmonic metal NPs themselves can also induce the catalysis directly.<sup>28</sup> In this case, plasmonic NPs are not only the photo-active components, but also are the catalytic-active species. The integration of plasmonic and catalytic properties into metallic NPs paves a new way for visible light-driven photocatalysis, and has shown great potential in selective organic transformations in a mild manner.<sup>8,29–31</sup>

As a new and burgeoning field, plasmon-mediated photocatalysis has been paid immense research interest.<sup>32–40</sup> In the present review, we mainly focus on the very recent advances and emerging strategies in harnessing single-active plasmonic nanostructures to enhance their catalytic properties with visible light excitation. Herein, the term “single-active” means that the plasmonic metallic nanostructures are the only photo- and catalytic-active material under visible light. In this context, plasmonic systems without photocatalytic applications, metal/semiconductor hybrids that employ plasmonic metal NPs to sensitize and/or improve the photocatalysis of the semiconductors,<sup>32–38</sup> and bi-metals plasmonic systems<sup>41,42</sup> will not be covered. This review starts with a brief introduction of LSPR phenomenon, and then focus on the plasmonic nanostructures including metals and doped-semiconductors, together with the parameters influencing their plasmonic frequencies. Subsequently, the surface plasmon decay process will be discussed. We concentrate the predominant attention in the plasmon-enhanced photocatalysis by single-active nanostructures, which fall into six categories concerning their existing forms, and try to highlight the underlying structure-function relationship. At last it ends with the summary and future outlook in developing highly efficient plasmon-mediated photocatalysis with visible light.

## 2. Plasmonic nanostructures

LSPR is a unique characteristic of metallic nanostructures, which is established when their particles sizes are comparable to or smaller than the wavelength of the incident light. Upon light illumination, the polarization of the free electron cloud gives rise to the accumulated negatively charged centers against the positive nucleus, creating an electric dipole (Fig. 1). The curved surface of metal NPs exerts an effective restoring force on the driven electrons, so that a resonance occurs, leading to the field enhancement both inside and in the near-field zone outside the NPs.<sup>43,44</sup> The enhancement attenuates quickly with distance from the surface, and the optical extinction cross section (sum of both absorption and scattering processes) of

metal NPs reaches a maximum at the plasmon resonant frequency.

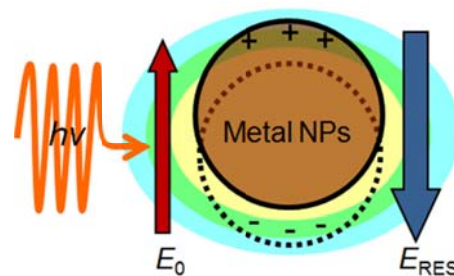


Fig. 1 The schematic illustration of LSPR excitation on metallic NPs.

In principle, due to the presence of free electrons in large quantities, most metal NPs could support LSPR in a wide range from UV to visible light region, such as Na,<sup>45</sup> K,<sup>45</sup> Al,<sup>46</sup> Co,<sup>47</sup> Pt<sup>48</sup> and Pd.<sup>48,49</sup> However, these metals suffer from the short plasmonic wavelengths in deep UV region or the instability to air/moisture. In terms of strong visible light response, noble metals of Au, Ag and Cu are suitable candidates.<sup>10,11,50–56</sup> For example, spherical Ag (38 nm in mean diameter), Au (25 nm) and Cu (133 nm) NPs exhibit LSPR absorption peaks at approximately 420, 520 and 610 nm, respectively, which are all located in the visible range (Fig. 2a).<sup>8</sup> In particular, Au and Ag NPs with higher chemical stability to oxidation and relatively more free electrons concentration (around  $5.9 \times 10^{22} \text{ cm}^{-3}$ ),<sup>57</sup> providing very intense and narrow absorption at lower wavelength of the visible range, are more attractive for solar utilization.

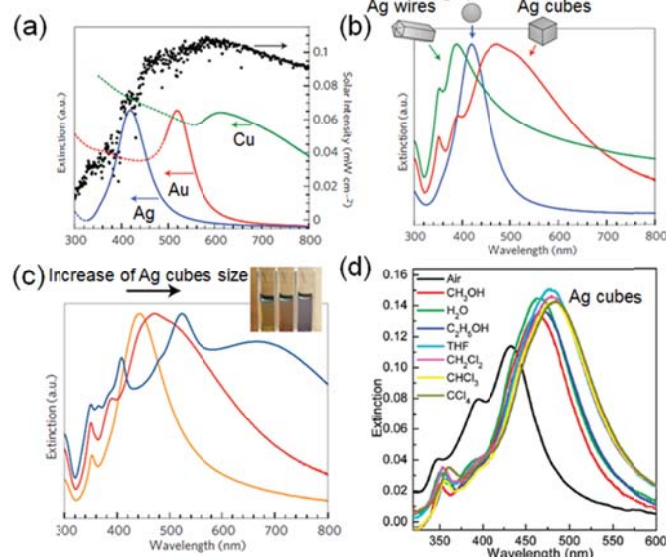
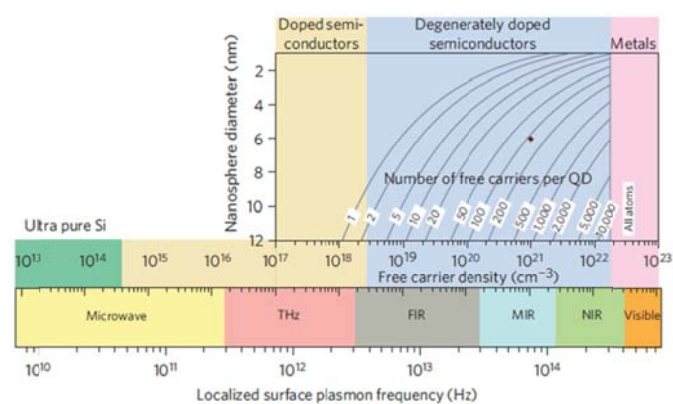


Fig. 2 The plasmonic wavelength dependence of metal nanostructures on their (a) metal species, (b) shapes and (c) sizes. Adapted with permission from ref. 8. Copyright 2011 Nature Publishing Group. (d) The effect of surrounding mediums on the plasmonic wavelength of Ag nanocubes. Adapted with permission from ref. 58. Copyright 2012 American Chemical Society.

The LSPR wavelength and intensity of metallic nanostructures are not only dependent on the nature of metals, but also on their shapes, sizes as well as the surrounding mediums.<sup>8,51,58</sup> The geometrical symmetry of metallic nanostructures determines their polarization modes, thereby leading to the number change of the observed LSPR peaks. The evolution of shapes from spheres into wires or cubes changes the LSPR wavelengths of Ag nanostructures, and also increases the number of LSPR peaks from one to two and three, respectively (Fig. 2b).<sup>8</sup> The increase in size will cause the LSPR wavelength of metal NPs to shift to longer wavelength (red shift, Fig. 2c). In addition, the LSPR wavelength also changes with the surrounding mediums due to their dielectric constant variation. When the surrounding environments changed from air to different solvents, LSPR wavelength of Ag nanocubes were found to red shifted as the surrounding refractive index of the solvent increased (Fig. 2d).<sup>58</sup>



**Fig. 3** The schematic diagram exhibiting the plasmonic frequency dependence on the free carrier density and doping constraints in metals and doped semiconductors. Reproduced with permission from ref. 60. Copyright 2011 Nature Publishing Group.

Recently, it has been revealed that LSPR can also occur in some highly-doped semiconductors, involving indium tin oxides (ITO),<sup>59</sup> copper chalcogenides ( $\text{Cu}_{2-x}\text{S}$ ),<sup>60–63</sup> transition-metal oxides ( $\text{TiO}_2$ ,  $\text{WO}_{3-x}$ ,  $\text{MoO}_{3-x}$ )<sup>64–68</sup> and many others.<sup>69–71</sup> As illustrated in Fig. 3, the sufficient free electrons concentration ( $10^{22}$ – $10^{23} \text{ cm}^{-3}$ ) enables metals to display LSPR absorption over a wide range from UV to visible light, and even to near infrared (NIR) region. However, in semiconductors, in order to sustain the LSPR high density of free carriers are introduced by doping.<sup>69,70</sup> As a consequence, the concentration of free carriers in doped-semiconductors is usually lower than  $10^{22} \text{ cm}^{-3}$ , resulting in their LSPR absorption at longer wavelength beyond the visible region. Such NIR absorption is extremely useful for applications in photothermal therapy and bio-imaging, where the interaction of tissue with light at these wavelengths is relatively weak.<sup>70</sup> Given the generation pathways for free charge carriers, plasmonic semiconductors can be generally divided into two categories, being extrinsic doping of the heterovalent atoms (e.g., ITO) and self-doping of

non-stoichiometric semiconductors through formation of oxygen or cation vacancies (e.g.,  $\text{WO}_{3-x}$ ,  $\text{Cu}_{2-x}\text{S}$ ).

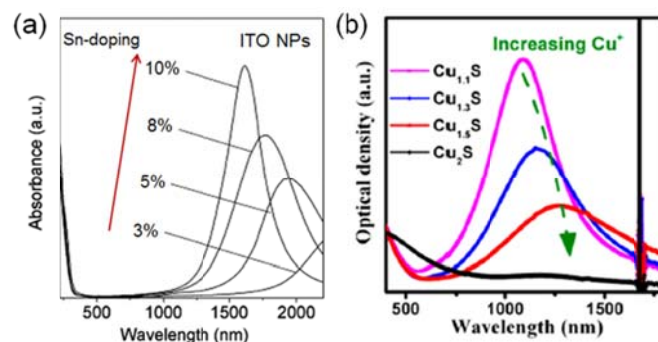


**Fig. 4** (a) The blue shift in the extinction spectra of ITO NPs with increasing Sn doping. Adapted with permission from ref. 59. Copyright 2009 American Chemical Society. (b) The red shift in the optical extinction spectra of  $\text{Cu}_{2-x}\text{S}$  NPs with increasing  $\text{Cu}^+$  concentration. Reproduced with permission from ref. 63. Copyright 2013 American Chemical Society.

Besides the effects of shapes, sizes and surrounding mediums that are analogous to noble metals, one additional feature of the doped-semiconductors is that their plasmonic frequencies could be tailored by changing the dopant concentrations, stoichiometric compositions or phase transitions.<sup>69,70</sup> For example, the introduction of Sn (IV) atoms into the  $\text{In}_2\text{O}_3$  lattice will lead to free charge carriers that are responsible for the conductivity, and considerable high concentration of free carriers could be expected to support LSPR in ITO NPs. Through controlling the Sn concentration from 3 to 10 mol%, the LSPR in the ITO NPs was blue shifted from  $>2200 \text{ nm}$  to  $1618 \text{ nm}$  (Fig. 4a).<sup>59</sup> Furthermore, in contrast with the stoichiometric semiconductors, the presence of cation or oxygen vacancies in non-stoichiometric counterparts could offer appreciable free carriers (electrons or holes) to support their LSPR. In the case of  $\text{Cu}_{2-x}\text{S}$ , as the copper vacancies gradually decreased from  $\text{Cu}_{1.1}\text{S}$  ( $x = 0.9$ ) to  $\text{Cu}_2\text{S}$  ( $x = 0$ ), the plasmonic absorption of  $\text{Cu}_{2-x}\text{S}$  NPs was red shifted to longer wavelength, and finally vanished for the stoichiometric  $\text{Cu}_2\text{S}$  (Fig. 4b).<sup>63</sup>

Arising from the strong light-matter interaction, LSPR enables metallic nanostructures to harvest the light efficiently. The plasmonic resonance frequencies are determined by the concentration of free carriers (electrons or holes), which is further dependent on an array of factors involving particle sizes, geometrical shapes and surrounding dielectric materials. Through rational manipulation of the metallic nanostructures, it is reasonable for one to tailor the corresponding plasmonic resonance in a wide range to absorb as much sunlight as possible.

### 3. Plasmon-enhanced photocatalysis

Upon resonant excitation, the electromagnetic field in the vicinity of plasmonic metal NPs will be enhanced. Through the finite-difference time-domain (FDTD) simulations, it shows

that the electric field intensity of the local plasmonic hot spots could reach as 1000 times high as that of the far-field incident light.<sup>35,72</sup> The decay of surface plasmons takes place on a femtosecond timescale either through radiative re-emission of photons, or non-radiative transfer of energy to hot electrons (Fig. 5).<sup>57</sup> In the non-radiative process, the energetic electrons will generally be injected to the nearby semiconductors to overcome the interfacial Schottky barrier,<sup>32–38,73</sup> or into the lowest unoccupied molecular orbital (LUMO) of the adsorbates,<sup>8,36</sup> thereby activating and stimulating the catalytic redox reactions. In addition to charge transfer, plasmonic heating can also occur as a result of electron-electron interaction and the subsequent thermalization.<sup>57</sup> In plasmonic metal NPs, the electron injection (within 50 fs) was found to be prior or simultaneous to the electron-electron scattering relaxation (<100 fs).<sup>74</sup> Both the hot electron transfer and thermal heating processes brought by surface plasmons of the metallic NPs are favorable for chemical reactions of the adsorbates, leading to the plasmon-enhanced photocatalysis.

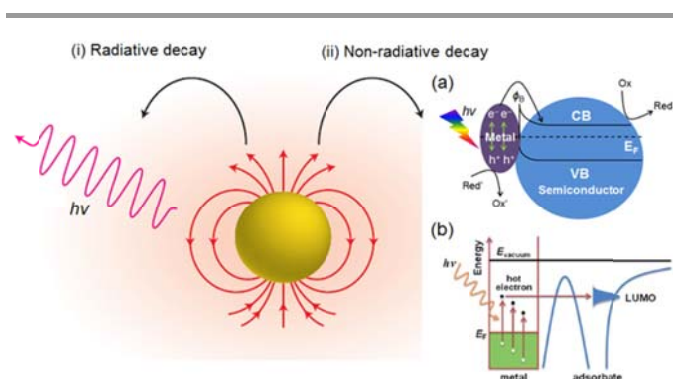


**Fig. 5** The schematic illustration of the surface plasmon decay process via (i) radiative and (ii) non-radiative routes. Adapted with permission from ref. 57. Copyright 2014 Nature Publishing Group. (a) The transfer of the hot electrons to the nearby semiconductor (n-type). Adapted with permission from ref. 73. Copyright 2013 Royal Society of Chemistry. (b) The direct injection of the hot electrons to the LUMO of the adsorbates. Reproduced with permission from ref. 36. Copyright 2013 Royal Society of Chemistry.

In single-active plasmonic catalysts, the metallic NPs perform as both the photo-sensitive and catalytic-active sites. Considering the existing forms that are used in photocatalysis, herein single-active plasmonic photocatalysts fall primarily into the following categories: (i) free-standing metals, (ii) metal/insulator hybrids, (iii) metal/WBG semiconductor hybrids, (iv) metal/carbon-based hybrids, (v) supported metal films and (vi) highly-doped semiconductor materials.

### 3.1 Free-standing metal catalysts

In plasmon-mediated single-active catalysis, plasmonic NPs are the sole photo- and catalytic-active sites rather than the support materials. Therefore, the free-standing plasmonic metal NPs without supports could be a compelling system to understand their intrinsic catalytic property and rule out the support-effect.<sup>75</sup> In contrast to Ag and Cu, Au NPs are more chemically

resistant and stable to oxygen atmosphere, thus making free-standing Au NPs suitable for direct plasmonic photocatalysis.

The first example of free-standing Au NPs as plasmonic photocatalysts was reported by Scaiano *et al.*<sup>76</sup> Colloidal Au NPs with sizes of ~15 nm was obtained by a solution-based photochemical method, and could oxidize alcohols into the corresponding carbonyl compounds with H<sub>2</sub>O<sub>2</sub> upon irradiation with either laser (532 nm) or LED (530 nm) light (eqn(1)). The Au NPs exhibited strong light absorption in visible region with LSPR peak of around 522 nm (Fig. 6a). Under LED illumination, plasmonic excitation of Au NPs was necessary to obtain substantial conversion of benzylic alcohols to the oxidized products, which was much higher than the cases without Au NPs (Fig. 6b).

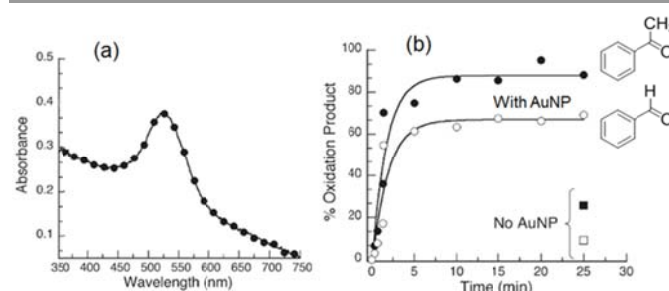
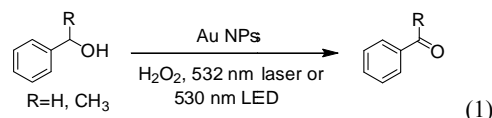
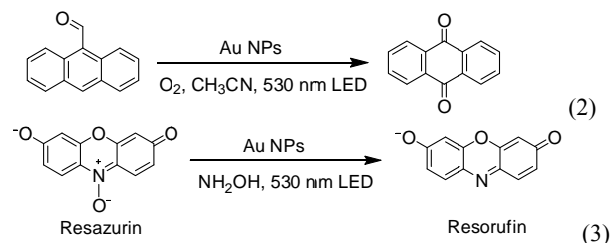


**Fig. 6** (a) UV-Vis spectra of colloidal Au NPs suspension in sec-phenethyl alcohol and H<sub>2</sub>O<sub>2</sub>. (b) Acetophenone and benzaldehyde yield as a function of LED excitation time with or without Au NPs. Adapted with permission from ref. 76. Copyright 2011 American Chemical Society.

Furthermore, in the presence of air or oxygen, Au NPs could promote the oxidation of 9-anthraldehyde to the predominant product anthraquinone in acetonitrile under 530 nm LED irradiation (eqn(2)).<sup>77</sup> The reaction did not occur in dark condition or without Au NPs, suggesting the catalysis triggered by Au NPs under plasmonic stimulation. With the aid of single particle detection technique, it was revealed that the dynamics of the surface plasmon mediated reactions involved Au NPs. Apart from oxidation reactions, Au NPs were also found to exhibit high efficiency in the reduction of resazurin into resorufin with hydroxylamine and green LED light (eqn(3)).<sup>78</sup>



### 3.2 Metal/inert insulator hybrids

Despite the fact that free-standing plasmonic metal NPs show considerable photocatalytic activity in organic

transformations under visible light irradiation, they are not desirable candidates for large-scale implementation. In typical photocatalytic conditions, the free-standing metal NPs are vulnerable to aggregation, and suffer from the low stability.<sup>76</sup> Therefore, from the point of view of practical applications plasmonic metal catalysts are usually supported on the solid oxide materials, which entail large surfaces to disperse the plasmonic NPs evenly and enable their recycled usage. One important class of the solid supports is the insulating oxides with band gaps over 5 eV,<sup>79</sup> for instance, ZrO<sub>2</sub> (~5.8 eV), SiO<sub>2</sub> (~9.0 eV) and Al<sub>2</sub>O<sub>3</sub> (~8.7 eV), which are unable to be excited by visible light (less than 3 eV). Besides, it is also difficult for the inert insulators to capture the hot electrons induced by the plasmonic metal NPs because of their large potential barrier.<sup>74,80</sup> Under this circumstance, the corresponding photocatalytic reactions exclude the participation of inert insulators.

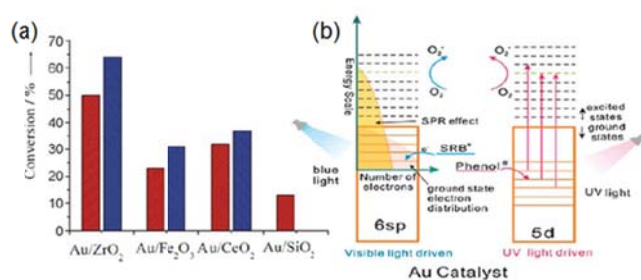
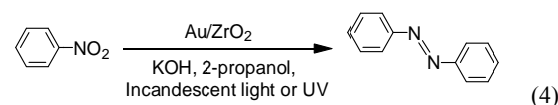


Fig. 7 (a) Photocatalytic decomposition of HCHO to CO<sub>2</sub> under blue light (blue bars) and red light (red bars) for Au NPs on the different oxide supports. Reproduced with permission from ref. 28. Copyright 2008 Wiley-VCH. (b) The schematic diagram of band structures for the supported Au NPs and the possible photocatalytic mechanism. Reproduced with permission from ref. 81. Copyright 2009 Royal Society of Chemistry.

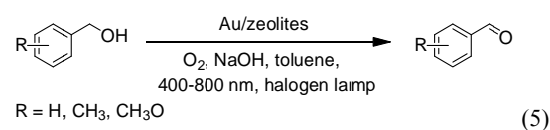
Triggered by their extraordinary catalytic properties, supported Au NPs on inert insulators as plasmonic photocatalysts have been paid much interest in the past several years.<sup>28,29,81–84</sup> In 2008, Zhu *et al.* first observed the oxidation of volatile organic compound (VOC) HCHO to CO<sub>2</sub> product by Au NPs supported on inert ZrO<sub>2</sub> and SiO<sub>2</sub>.<sup>28</sup> Fig. 7a displays the HCHO decomposition over a range of supported Au photocatalysts under blue (400–500 nm) or red (600–700 nm) light illumination. Although visible-light-sensitive semiconductors (Fe<sub>2</sub>O<sub>3</sub>) supported Au NPs showed higher efficiency, the photocatalysis with Au NPs on optically inert SiO<sub>2</sub> was found to be active under red light irradiation, giving clear evidence for plasmon-driven chemical reactions with visible light. Furthermore, organic dye molecules, such as sulforhodamine-B (SRB) and methyl orange (MO), could be degraded over supported Au catalysts on a range of insulating oxides (ZrO<sub>2</sub>, SiO<sub>2</sub>, zeolites and halloysite) under visible light irradiation.<sup>81–83</sup> The photocatalytic activity of Au NPs on supported insulators was attributed to be electronic effect in nature, as depicted in Fig. 7b. For Au NPs, the transition of 5d electrons to 6sp band (interband transition) causes considerable

UV absorption.<sup>81</sup> In addition, the plasmonic resonance of Au NPs originates from the intraband transition of their 6sp electrons, leading to the visible light absorption. Under visible light illumination, the electrons of Au NPs gain energy through plasmonic resonance and migrate to higher potential intraband levels, where they are then captured by the oxygen molecules, leaving Au NPs with positive charges. To maintain the electric charge neutrality, Au NPs will seize the electrons from the adsorbed organic molecules, thereby oxidizing these organic compounds.

In contrast with complete decomposition of organic macromolecules into small inorganic species, for example CO<sub>2</sub> and H<sub>2</sub>O, selective organic transformation into desirable products holds much greater prospects for both scientific researches and industrial applications. For instance, Zhu *et al.* reported the visible light driven reduction of nitrobenzene to azobenzene on Au/ZrO<sub>2</sub> catalysts with high efficiency (eqn(4)).<sup>29</sup> With sizes of about 6 nm and LSPR peak around 520 nm, Au NPs was supported on ZrO<sub>2</sub> by the reduction-deposition method with NaBH<sub>4</sub> in the presence of lysine. It was noted that the plasmon-driven catalytic reactions could show high selectivity at low temperature and pressure, outperforming the conventional thermal catalysis with higher reaction temperature and lower product selectivity. In addition, photocatalytic reduction of styrene oxide into the styrene product has also been executed over insulating oxides (ZrO<sub>2</sub>, Al<sub>2</sub>O<sub>3</sub> and zeolite-Y) supported Au NPs, showing good selectivity under visible light irradiation.<sup>84</sup>



Selective oxidation of alcohols by Au NPs has been widely studied in organic synthesis, in which the resulting carbonyl products perform as important industrial intermediates.<sup>85</sup> As a rule, benzyl alcohol is used as a reference for selective oxidation reactions. Au NPs supported on insulating zeolites can serve as plasmonic photocatalysts for aerobic oxidation of benzyl alcohol in toluene under illumination of visible light from a 500 W halogen lamp (Eqn(5)).<sup>86</sup> It was found that Au/zeolite photocatalysts could oxidize aromatic alcohols into the corresponding aldehydes with high conversion under visible light irradiation, while in the dark condition the reactions proceeded with much lower conversion rate. The conversion efficiency was observed to be dependent on the supports, with the Au/zeolite-Y catalyst performing the best. Other inert materials, such as Al<sub>2</sub>O<sub>3</sub> and hydrotalcite, have also been used as solid supports for Au NPs. Upon irradiation with the 530 nm LED light source, the Au/Al<sub>2</sub>O<sub>3</sub> and Au/hydrotalcite catalysts displayed considerable efficiency towards selective oxidation of benzyl alcohol in the presence of H<sub>2</sub>O<sub>2</sub>.<sup>87</sup>



As the versatile starting substrates, aromatic amines and ester derivatives play vital roles in the synthesis of complicated pharmaceutical molecules. Recently, it has been shown that the chemical production of such derivatives could take place by plasmonic Au catalysts under visible light.<sup>88,89</sup> Through a tandem oxidation/amidation process between benzaldehyde and morpholine with H<sub>2</sub>O<sub>2</sub> in basic KOH condition, 4-benzoylmorpholine was obtained over the Au/SiO<sub>2</sub> catalyst under 532 nm laser illumination (eqn(6)).<sup>88</sup> Because selective oxidation of alcohols into aldehydes was easy to proceed in the same condition, the amide formation could also occur by using benzyl alcohol as the starting material. In addition, visible light could drive the esterification from aldehydes and alcohols on supported Au NPs (Au/ $\gamma$ -Al<sub>2</sub>O<sub>3</sub>) photocatalysts (eqn(7)).<sup>89</sup> The photocatalytic activity was found to be related to the light intensity and wavelength, elucidating the plasmon-enhanced photocatalysis by Au NPs.

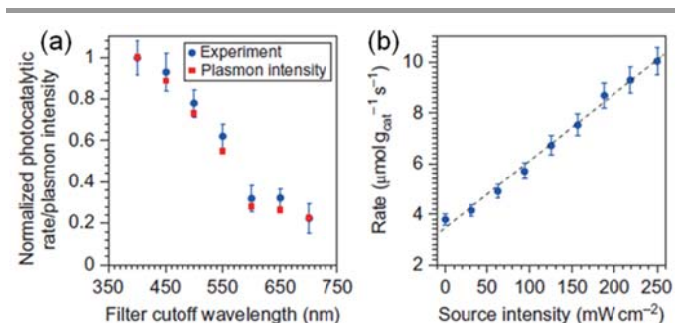
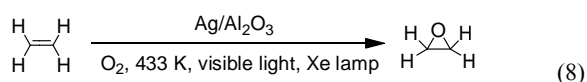
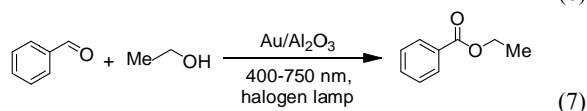
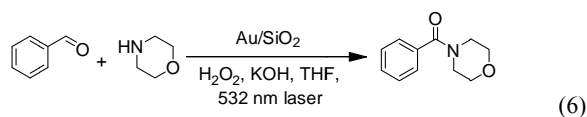


Fig. 8 (a) Wavelength- and (b) intensity-dependent photocatalytic activity of Ag/Al<sub>2</sub>O<sub>3</sub> catalysts in the photocatalytic ethylene epoxidation under visible light irradiation. Reproduced with permission from ref. 30. Copyright 2011 Nature Publishing Group.

Analogous to Au, Ag and Cu NPs are also important visible-light-responsive plasmonic metal catalysts. As one commercially pivotal reaction, selective epoxidation of ethane to ethylene oxide has been executed on supported Ag nanostructures (Ag/ $\alpha$ -Al<sub>2</sub>O<sub>3</sub>) using low intensity visible light and thermal energy (eqn(8)).<sup>30,90</sup> Ag nanocubes with the edge length of about 60 nm were supported on the  $\alpha$ -Al<sub>2</sub>O<sub>3</sub> surface, showing the plasmonic peak wavelength of *ca.* 400 nm. The observed reaction rate of ethane epoxidation conducting at 433 K with low intensity visible light (250 mW cm<sup>-2</sup>) irradiation was comparable to that at 473 K in the dark condition, which

demonstrates a unique route towards enhanced selective chemical reactions by plasmonic Ag nanocatalysts. As shown in Fig. 8, the measured photocatalytic rate matched well with the plasmon intensity, while there was a linear relationship between the photocatalytic activity and the intensity of incident light source. The presence of such linear dependence indicates that the energetic electrons, mediated by the excitation of surface plasmons in Ag nanocubes, were responsible for the photoactivity. Furthermore, kinetic studies using labelled <sup>18</sup>O<sub>2</sub> exhibited a larger kinetic isotope effect (KIE) value for photothermal process (1.19±0.01) with respect to that of thermal process (1.06±0.02). Thus, the surface plasmon-induced energetic electrons on irradiated Ag NPs were transferred to the adsorbed molecular O<sub>2</sub>, accelerating its dissociation process. Moreover, supported Ag NPs on inert oxides (Ag/zeolite-Y, Ag/ZrO<sub>2</sub>, Ag/SiO<sub>2</sub>) also showed good photocatalytic activity in degradation of organic dyes, such as SRB and methylene blue (MB).<sup>91,92</sup> Through plasmonic excitation of 5*sp* electrons, the supported Ag NPs even surpassed N-doped TiO<sub>2</sub> in oxidation of the organic molecules under visible light irradiation.<sup>91</sup>

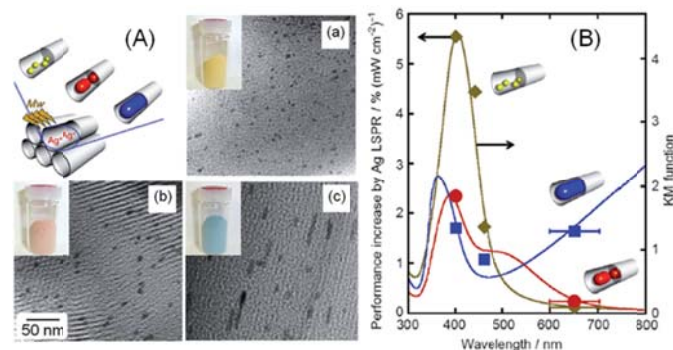
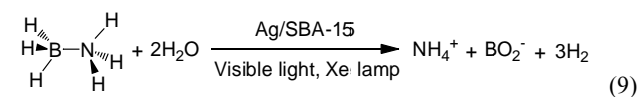


Fig. 9 (A) TEM images and photographs of the Ag/SBA-15 hybrids with different sizes of Ag NPs. (B) The action spectra of the enhanced catalytic performance for the Ag/SBA-15 hybrids. Adapted with permission from ref. 94. Copyright 2013 Wiley-VCH.

The quest for high-quality hydrogen storage and release systems is indispensable to modern on-board applications, such as proton exchange membrane fuel cell (PEMFC). Ammonia borane (NH<sub>3</sub>BH<sub>3</sub>), which contains as high as 19.6 wt% hydrogen and exceeds that of gasoline, is an attractive and potential target.<sup>93</sup> Recently, plasmon-enhanced catalysis from NH<sub>3</sub>BH<sub>3</sub> dehydrogenation has been demonstrated on the mesoporous silica (SBA-15) supported Ag NPs under visible light irradiation (eqn(9)).<sup>94</sup> The Ag/SBA-15 hybrid was prepared by the microwave-assisted alcohol reduction method, in which Ag NPs having different sizes were obtained by controlling the irradiation time of microwave (3 or 5 min) and the usage of surface ligand (sodium laurate). As shown in Fig. 9

of the transmission electron microscopy (TEM) images, the Ag/SBA-15 samples with different sizes of Ag NPs exhibited different colours: (a) small NPs with yellow colour, (b) short nanorods with red colour, and (c) long nanorods with blue colour, which were also reflected by their different LSPR absorption in the UV–Vis spectra. The supported Ag NPs showed enhanced H<sub>2</sub> generation rate for NH<sub>3</sub>BH<sub>3</sub> dehydrogenation under visible light (>420 nm) irradiation compared to that conducted in dark condition. The enhancement for initial H<sub>2</sub> yield was dependent on the sizes of Ag NPs, with larger Ag NPs showing greater activity improvement. The rates of the enhanced catalytic performances by different wavelength were almost consistent with the LSPR absorption of Ag NPs, supporting the hypothesis that the enhanced catalytic property was derived from the plasmonic effect of Ag NPs.

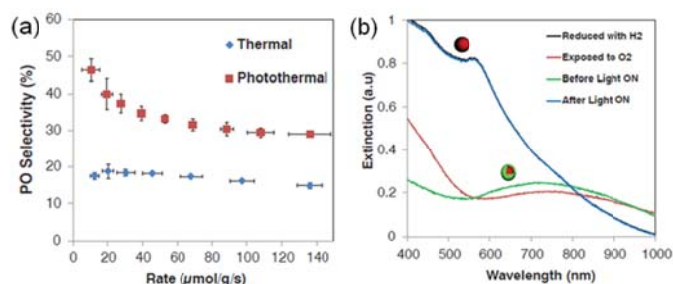
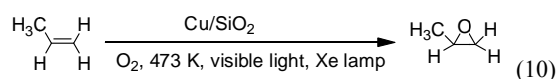


Fig. 10 (a) The selectivity to propylene oxide for thermal (light off) and photothermal (light on) processes as a function of the reaction rate. (b) *In situ* diffuse reflectance UV–Vis extinction spectra of the Cu/SiO<sub>2</sub> catalyst treated under different conditions. Adapted with permission from ref. 31. Copyright 2013 American Association for the Advancement of Science.

Copper metal is prone to surface oxidation upon exposure to ambient atmosphere, hence the employment of Cu NPs as plasmonic catalysts have not been paid much attention relative to Au and Ag. Nevertheless, one of the pioneering studies using Cu NPs for plasmonic catalysis has recently been reported by Linic *et al.*<sup>31</sup> The Cu NPs with an average size of 41 nm supported on inert SiO<sub>2</sub> was prepared by a solution reduction method with hydrazine, which was used to catalyze the propylene epoxidation under visible light (eqn(10)). Interestingly, the selectivity of the propylene oxide product changed from 20% (in dark condition) to nearly 50% (under visible light irradiation), showing the light irradiation-induced selectivity increase (Fig. 10a). The sharp increase in selectivity was found to be accompanied by the light-induced reduction of the surface Cu atoms (Fig. 10b). Prior to light irradiation, the Cu catalysts were oxidized to Cu@Cu<sub>2</sub>O structures with Cu<sub>2</sub>O shell covering the metallic Cu core. Subsequent illumination of the catalysts with visible light led to the reduction of the Cu<sub>2</sub>O shell, manifested by the appearance of the plasmonic absorption of metallic Cu NPs around 565 nm. It was believed that Cu NPs with the oxidized Cu<sub>2</sub>O shell absorb visible light to induce

plasmon excitation, and then the plasmonic hot electrons would weaken and break the Cu–O bonds, facilitating the reduction of Cu<sub>2</sub>O to Cu.<sup>31</sup> This finding sheds some light on the potential use of the unstable plasmonic metallic nanostructures, allowing their efficient catalysis with the assistance of light.

### 3.3 Metal/WBG semiconductors hybrids

Besides the insulating oxides supports, WBG semiconductors, such as CeO<sub>2</sub> (3.19 eV),<sup>95</sup> TiO<sub>2</sub> (3.20 eV)<sup>96</sup> and ZnO (3.20 eV),<sup>96</sup> can also work as important supports for single-active plasmonic photocatalysts. Visible light irradiation (>400 nm) is inefficient to induce the band gap excitation of these WBG semiconductors. Nonetheless, there usually exists the Schottky barriers between noble metals (*e.g.*, Au) NPs and WBG semiconductors (*e.g.*, TiO<sub>2</sub>). Upon light illumination, the hot electrons from the excited noble metal NPs with energies above the Schottky barrier (~1.0 eV) will be injected into these WBG semiconductors, leading to direct charge separation on the plasmonic NPs.<sup>74,97–100</sup> In such a way, interfacial charge transfer can be realized between plasmonic metals and WBG semiconductor supports, further influencing their catalytic performance. However, in the case of the insulating oxides (*e.g.*, ZrO<sub>2</sub>), interfacial hot electron transfer from plasmonic NPs is impeded due to their large potential barriers.<sup>74</sup>

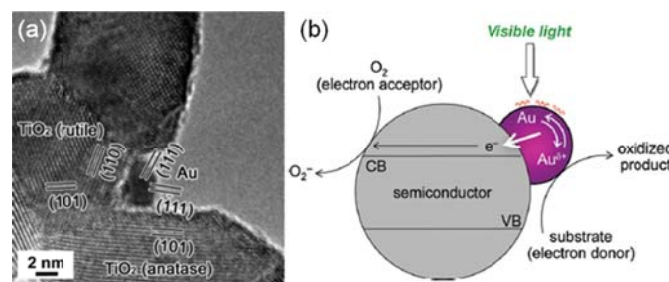
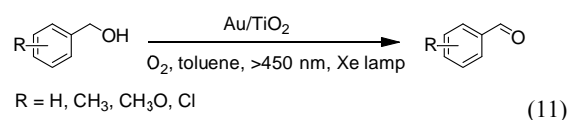
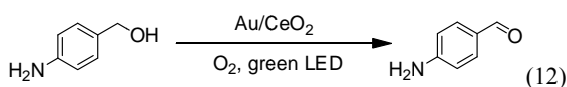


Fig. 11 (a) HRTEM image of Au/P25 TiO<sub>2</sub> hybrid and (b) Proposed mechanism for visible light driven aerobic oxidation by Au NPs supported on WBG semiconductors. Adapted with permission from ref. 105. Copyright 2012 American Chemical Society.

As one of the most studied semiconductors, TiO<sub>2</sub> has been found to exhibit efficient visible light photocatalytic performances with the addition of plasmonic Au NPs.<sup>19,20,22,24,26,98,99,101–104</sup> Furthermore, TiO<sub>2</sub> has also been employed to support Au NPs to promote the aerobic oxidation of alcohols under visible light.<sup>105,106</sup> For example, Au NPs loaded on P25 TiO<sub>2</sub> could enhance benzyl alcohol oxidation at room temperature with visible light (eqn(11)).<sup>105</sup> The Au/TiO<sub>2</sub> catalysts were prepared by the deposition-precipitation (DP) method. From the high resolution transmission electron microscopy (HRTEM) image, Au NPs with sizes less than 5 nm were found to locate at the anatase/rutile interface of P25 TiO<sub>2</sub> (Fig. 11a). The Au/TiO<sub>2</sub> hybrids, exhibiting a LSPR absorption

band at *ca.* 550 nm, showed high yield of the aldehyde or ketone products in toluene under visible light illumination (>450 nm). As evidenced by the electron spin resonance (ESR) spectra, electrons transferred from the plasmon-activated Au NPs to the adjacent TiO<sub>2</sub>, and ultimately was captured by the electron acceptors (O<sub>2</sub>). Meanwhile, the positively charged Au NPs were quenched by the alcohols, thus promoting their oxidation to complete the plasmonic resonance circle (Fig. 11b). The Au/TiO<sub>2</sub> was also active in the chemo-selective oxidation of alcohols in water with O<sub>2</sub> under visible light.<sup>106</sup> Based on the good resemblance of the action spectrum with optical absorption of the Au/TiO<sub>2</sub> catalysts, it was concluded that plasmonic excitation of Au NPs was the driving force for alcohol oxidation. In contrast, Au/ZrO<sub>2</sub> exhibited no activity under visible light because the conduction band (CB) position of ZrO<sub>2</sub> is too high for hot electrons on Au NPs to transfer.<sup>106</sup>

Au/CeO<sub>2</sub> catalysts have also been discovered to show high efficiency in photocatalytic selective oxidation of alcohols.<sup>107,108</sup> The Au/CeO<sub>2</sub> catalysts were prepared by photodeposition of HAuCl<sub>4</sub> on CeO<sub>2</sub> in the presence of citric acid. Under green laser irradiation with O<sub>2</sub>, alcohols were oxidized into the corresponding aldehydes in water on the Au/CeO<sub>2</sub> catalysts. The apparent quantum efficiency (AQE) was in agreement with the photoabsorption, and the highest value occurred at the LSPR wavelength (550 nm) of Au NPs. Subsequently, it was found that increasing Au NPs sizes resulted in enhanced catalytic activity of the Au/CeO<sub>2</sub> hybrids towards alcohol oxidation.<sup>107</sup> Multi-step photodeposition increased the sizes of Au NPs (~92 nm) relative to that (~59 nm) prepared by single-step method. Despite the presence of amine functional groups, Au/CeO<sub>2</sub> exhibited chemo-selective oxidation of 4-aminobenzyl alcohol to 4-aminobenzaldehyde under green laser light illumination (eqn(12)).<sup>108</sup> Larger Au NPs with stronger plasmonic absorption showed superior photocatalytic activity to smaller ones. In a recent study using paramagnetic resonance spectroscopy (EPR) measurement, it was revealed that the Au-H intermediates were important to alcohol oxidation by Au NPs under both UV and visible light irradiation.<sup>109</sup> This finding gives insight into the reaction processes of alcohol oxidation with Au catalysts, and may open up new possibilities to use alcohols as hydrogen donors for hydrogenation reactions.



Plasmon-assisted selective oxidation reactions by supported Au NPs are not limited to aerobic oxidation of alcohols, but are also shown in other reactions, such as oxidation of thiol,<sup>110</sup> benzene<sup>111–113</sup> and amines.<sup>114</sup> Selective oxidation of thiol to disulfide has been found to be achievable on TiO<sub>2</sub> supported Au NPs under visible light (eqn(13)).<sup>110</sup> The Au/TiO<sub>2</sub> was prepared by the DP method, and showed a broad LSPR absorption around 550 nm. Under visible light irradiation (>420 nm), Au/TiO<sub>2</sub> could catalyze the oxidation of thiol to disulfide in the presence of O<sub>2</sub>. Interestingly, the reaction was reversed with

UV light irradiation (>300 nm) from disulfide to thiol. The different electron transfer processes under visible light and UV light induced different reaction directions on the Au/TiO<sub>2</sub> catalyst. As a rather stable compound, benzene has been found to be transformed into phenol with the supported Au photocatalysts in the presence of oxidative atmosphere (O<sub>2</sub> or CO<sub>2</sub>) under visible light (eqn(14)).<sup>111–113</sup> For example, an *in situ* method was used to prepare metal NPs (Au, Ag and Pt) anchored on TiO<sub>2</sub> microsphere, in which metal precursors were reduced by the produced surface Ti<sup>3+</sup> ions of TiO<sub>2</sub> particles.<sup>113</sup> The obtained Au/TiO<sub>2</sub> and Ag/TiO<sub>2</sub> displayed clear plasmonic absorption peaks at approximately 540 and 450 nm, respectively (Fig. 12a). Under visible light irradiation, benzene oxidation into phenol in the presence of O<sub>2</sub> was observed on TiO<sub>2</sub> supported metal NPs, with the highest activity obtaining on Au/TiO<sub>2</sub> (Fig. 12b). Au/TiO<sub>2</sub> catalyst also showed visible light activity for amines oxidation to the corresponding imines (eqn(15)).<sup>114</sup> The Au/TiO<sub>2</sub>, with Au NPs of about 7 nm on the rutile TiO<sub>2</sub> particles, was prepared by the DP method. A range of oxide materials (TiO<sub>2</sub>, SrTiO<sub>3</sub>, ZnO, WO<sub>3</sub>, In<sub>2</sub>O<sub>3</sub> and Nb<sub>2</sub>O<sub>5</sub>) were employed as supports, while Au/rutile TiO<sub>2</sub> showed the best photocatalytic performance towards amines oxidation under visible light. In these reactions, LSPR-induced electrons transferred from Au NPs to TiO<sub>2</sub> lowers the Fermi level of Au NPs, thereby entailing their oxidation ability. Thanks to the wild oxidation ability of Au NPs, selective oxidation of thiol to disulfide, benzene to phenol and amines to imines could proceed without further overoxidation.

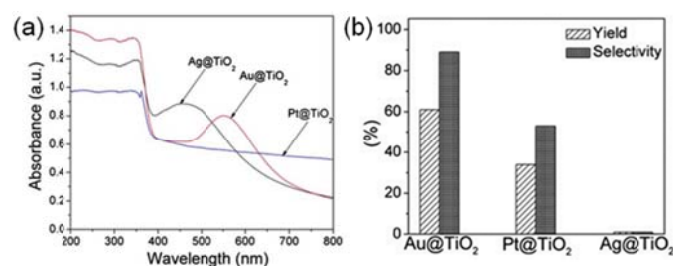
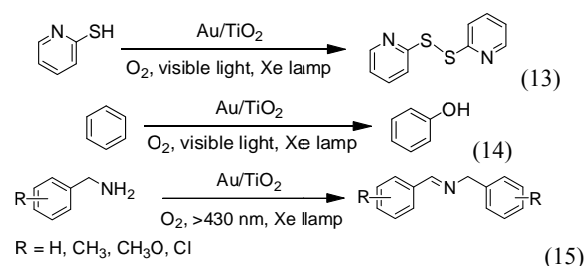


Fig. 12 (a) UV-Vis spectra of M@TiO<sub>2</sub> (M = Au, Ag, Pt), and (b) The yield and selectivity of phenol product over different photocatalysts. Reproduced with permission from ref. 113. Copyright 2011 Royal Society of Chemistry.

Visible light-driven reduction reaction was also boosted on WBG semiconductors supported Au NPs. Au/CeO<sub>2</sub> catalysts were found to be efficient in the selective reduction of organic compounds, including deoxygenation of epoxides to alkenes, reduction of ketones to alcohols and hydrogenation of azobenzene to hydrazobenzene, with visible light at ambient

condition (eqn(16)).<sup>115</sup> It was observed that the reduction ability of the Au/CeO<sub>2</sub> catalysts could be tailored by choosing the irradiation light wavelength. The shorter light wavelength endows Au/CeO<sub>2</sub> with greater reduction power of conduction electrons, thereby driving much harsher catalytic reactions. This offers a design protocol to manipulate selective chemical synthesis through plasmonic excitation of metal NPs with tunable light irradiation wavelength. In a recent study, TiO<sub>2</sub> supported Au NPs showed significant enhancement in photocatalytic reduction of nitrobenzenes to azobenzenes upon visible light irradiation (eqn(17)).<sup>116</sup> The Au/TiO<sub>2</sub> catalysts, having Au NPs with a bimodal distribution of both small (2.1 nm) and large (9.0 nm) sizes, were prepared by a two-step method and showed broad absorption in the visible light range with LSPR wavelength around 550 nm. Under visible light irradiation, the bimodal Au/TiO<sub>2</sub> exhibited highly enhanced catalytic performance towards nitrobenzenes reduction than that in the dark. In contrast, however, the unimodal Au/TiO<sub>2</sub>, which contains only small or large sizes of Au NPs, was inactive under visible light. The high efficiency of the bimodal Au/TiO<sub>2</sub> was ascribed to the plasmon-induced electron transfer from small Au NPs to larger ones through CB of TiO<sub>2</sub> (Fig. 13). As a result, small Au NPs functioned as the oxidation sites for 2-propanol, while reduction of nitrobenzene took place on large Au NPs. Through plasmonic excitation of Au NPs, the neat one-directional charge separation led to the enhanced catalytic activity.

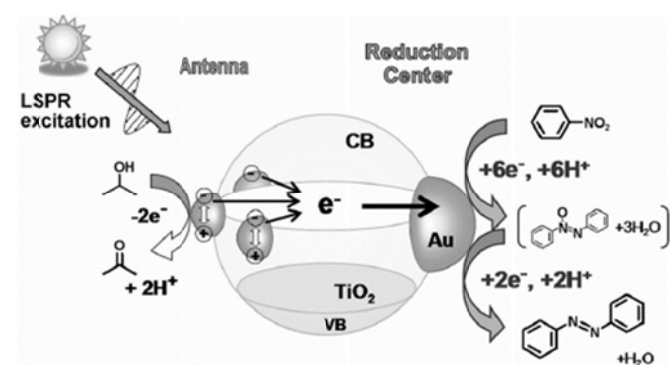
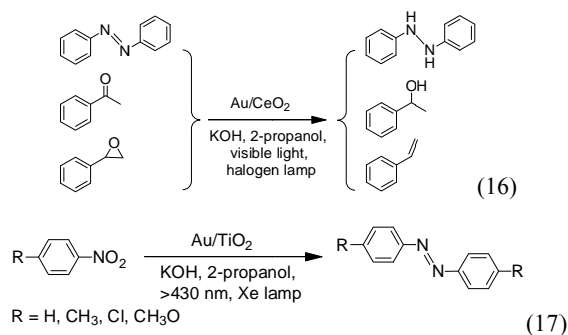
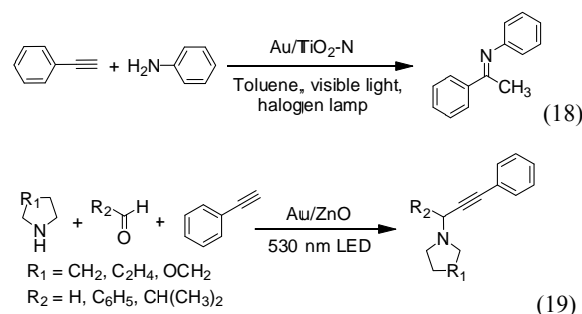


Fig. 13 The reaction mechanism for the visible light-induced electron transfer from small to large Au NPs in Au/TiO<sub>2</sub> catalysts. Reproduced with permission from ref. 116. Copyright 2014 Wiley-VCH.

Aromatic amines are important versatile intermediates for fine chemicals and organic synthesis in pharmaceutical industry. Recently, direct production of imines from hydroamination of alkynes with amines was achieved on supported Au NPs photocatalysts (Au/TiO<sub>2</sub>-N) under visible light (eqn(18)).<sup>117</sup> Without Au NPs or visible light irradiation, almost no reaction observed, indicating the role of plasmonic Au NPs as the catalytic sites. The TiO<sub>2</sub>-N support, which was endowed with rich Ti<sup>3+</sup> sites by N doping, provided more coordination sites for H addition and thus outperformed other supporting materials. As N doping introduces new gap states, the enhanced optical transitions involving mid-gap defect states could also contribute to the enhanced photocatalytic performance.<sup>118</sup> Plasmonic excitation of ZnO supported Au NPs can also induce selective formation of propargylamines from a mixture of an aldehyde, amine and phenylacetylene under 530 nm LED illumination (Eqn(19)).<sup>119</sup> It was found that in contrast to Al<sub>2</sub>O<sub>3</sub> and TiO<sub>2</sub> supports, ZnO could interact with alkyne and led to Au NPs-driven photocatalysis with the product yield as high as 95%.



Apart from the organic transformation reactions mentioned above, visible light irradiation could also expedite CO oxidation over supported Au NPs. Prepared by the DP method, Au/TiO<sub>2</sub> exhibited an LSPR absorption peak around 540 nm.<sup>120</sup> The introduction of visible light (490–780 nm) irradiation could boost the CO conversion compared to dark condition. It was proposed that LSPR effect favored the adsorption and activation of CO on the surface of Au NPs, thereby enhancing its oxidation. Further studies showed that CO oxidation was dependent on the electron transfer behavior between Au NPs and support materials.<sup>121</sup> Visible light could accelerate the adsorption and activation of CO over Au/TiO<sub>2</sub>, while suppressed its selectivity over Au/Al<sub>2</sub>O<sub>3</sub>. Upon plasmonic excitation, electrons were transferred from Au NPs to TiO<sub>2</sub> over Au/TiO<sub>2</sub>, yet in the case of Au/Al<sub>2</sub>O<sub>3</sub> such process was prohibited. This finding demonstrates that CO oxidation is dominated by the metal-support interaction, in which proper electron transfer could improve preferential oxidation of CO over the supported Au catalysts.

### 3.4 Metal/carbon-based hybrids

As one of the most abundant elements in the biosphere, carbon materials have shown great potential in the sustainable energy and environmental science. In recent years, the arising carbon

materials such as zero-dimensional (0D) fullerene (C<sub>60</sub>), one-dimensional (1D) carbon nanotubes (CNTs) and two-dimensional (2D) graphene, exhibit excellent electrical, optical and mechanical properties.<sup>122</sup> Carbon materials usually possess large surface area, good adsorption capacity as well as high electronic conductivity, which provide indispensable and protective supports to plasmonic nanocatalysts.<sup>123–125</sup>

Supported metal NPs on carbon materials have shown efficient activity in degradation of organic dyes under visible light. For example, amorphous carbon can be used as basis material to support and protect Ag NPs.<sup>126</sup> As displayed in Fig. 14, the Ag@C core@shell hybrid, which was composed of Ag cores of 70–100 nm and carbon shell with thickness around 25 nm, showed a broad LSPR absorption centering at 630 nm. The Ag@C hybrid displayed higher photocatalytic activity than that of N-TiO<sub>2</sub> in RhB degradation and gaseous CH<sub>3</sub>CHO decomposition under visible light, which was predominantly attributed to the plasmonic effect of Ag NPs.

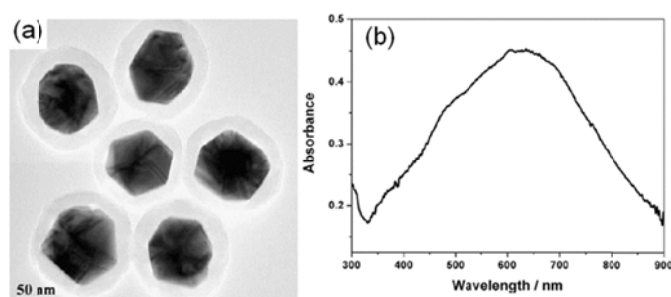


Fig. 14 (a) TEM image and (b) UV-Vis spectrum of the Ag@C hybrid dispersed in ethanol. Reproduced with permission from ref. 126. Copyright 2009 Elsevier B.V.

Graphene, a 2D network composed of monolayer sp<sup>2</sup>-hybridized carbon atoms, has been paid ever-growing interest due to its supreme and unique structural and electronic properties.<sup>127</sup> The presence of delocalized electrons, dangling bonds and carbon vacancies enables graphene to facilitate the interfacial charge transfer with plasmonic metal NPs and stabilize them. Hybrids of graphene and plasmonic metal NPs, such as Au/graphene<sup>128</sup> and Ag/graphene,<sup>129</sup> have shown excellent visible-light photocatalytic performance in degrading dyes solutions. With respect to conventional semiconductors, plasmonic metal/graphene hybrid possessed higher adsorption, stronger p-p interaction with dye chromophores, more efficient photosensitized electron injection and slower electron recombination, guaranteeing their superior photocatalytic activities.<sup>128</sup> In addition, graphene supported plasmonic NPs have recently exhibited efficient selective reduction of nitrobenzene under visible light.<sup>130</sup> The Cu/graphene hybrid was prepared by reduction of Cu<sub>2</sub>O/graphene composites in H<sub>2</sub> atmosphere at elevated temperature. As displayed in Fig. 15, the obtained Cu/graphene hybrid, with Cu NPs of about 15 nm dispersing on 2D graphene nanosheets, showed an LSPR absorption peak at around 560 nm. Under visible light irradiation, Cu/graphene exhibited highly enhanced performance and selectivity towards nitrobenzene reduction compared to that in dark condition. The wavelength-

dependence of the catalytic activity (Fig. 15b) suggested that the reaction was induced by plasmonic effect of Cu NPs. This work illustrates the hybridization with carbon materials could enable unstable metal NPs to be more resistant to oxidation.

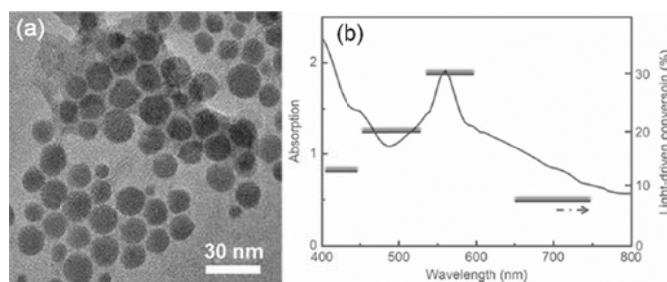
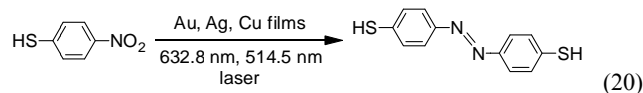


Fig. 15 (a) TEM image and (b) the action spectrum of photocatalytic activity for the Cu/graphene. Reproduced with permission from ref. 130. Copyright 2014 Wiley-VCH.

### 3.5 Supported metal films

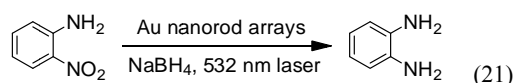
In heterogeneous photocatalysis, supported metal films demonstrate an immobilized system that allows easy recycle as well as long term use. Furthermore, the integration of plasmonic metals in films facilitates the chemical reactions for single-molecule detection and synthesis through remote SERS.<sup>12–14</sup> Thus, the construction of supported films expand the applications of plasmonic metals.

Supported metal films have been found to play a pivotal role in the plasmon-assisted surface-catalyzed reactions during SERS measurement, with the formation of 4,4'-dimercaptoazobenzene (DMAB) either by oxidation of 4-aminothiophenol (PATP) or reduction of 4-nitrobenzenethiolate (4NBT).<sup>131,132</sup> For instance, Sun *et al.* reported the use of plasmonic metal (Au, Ag, Cu) films for the reduction of 4NBT to DMAB under red and green laser irradiation (eqn(20)).<sup>132</sup> The Au, Ag, and Cu films with the average thickness of 50 nm were prepared by the vacuum electron beam evaporation. It was found that the reduction reaction was strongly dependent on the substrate, the laser wavelength and the reaction timescales, which could be rationally chosen to accelerate or restrain the reaction. A variety of supported plasmonic metal films, such as Au rings,<sup>133</sup> Ag NPs arrays,<sup>134</sup> Ag microspheres,<sup>135</sup> roughened Ag substrate<sup>136</sup> as well as Au and Ag NPs,<sup>137,138</sup> have been employed to understand the underlying mechanism of SERS. The introduction of LSPR effect not only drives the transfer of hot electrons to activate the chemical reaction, but also enhances Raman signal of the surface species.<sup>137</sup>



In addition to driving the surface-catalyzed reactions during SERS, enhanced performance in conventional catalysis have also been observed on the supported metal films with visible light irradiation.<sup>139,140</sup> For example, anisotropic Au nanorod arrays showed the plasmon-enhanced photocatalysis in reduction of 2-nitrobenzamine (eqn(21)).<sup>139</sup> The

unidirectional Au nanorod arrays with optical anisotropy was fabricated by the oblique angle deposition technique on a p-type silicon wafer. Under green laser light irradiation, these arrays displayed an obvious improvement in the catalytic reduction of 2-nitrobenzenamine to 1,2-benzenediamine with  $\text{NaBH}_4$ , which was assigned to the plasmonic effect of the Au nanorods.



### 3.6 Non-metal semiconductor plasmonic catalysts

Different from noble metals that possess abundant free electrons, in semiconductors high doping is required to satisfy the prerequisite for LSPR. Consequently, doped-semiconductors have lower carrier concentration than metals, and hence lower plasmonic frequencies in the NIR range. The longer LSPR wavelength absorption of the doped-semiconductors have rendered them appropriate candidates for bio-medical and optoelectronic applications.<sup>69,70</sup> For photocatalytic reactions, extrinsically-doped semiconductors are not suitable as the heterovalent atom sites facilitates the recombination of the photo-excited charge carriers. Nonetheless, it may become favourable for the self-doped non-stoichiometric semiconductors ( $\text{WO}_{3-x}$ ,  $\text{MoO}_{3-x}$ ,  $\text{Cu}_x\text{In}_y\text{S}_2$ , etc.), because the stoichiometric form of them have turned out to be efficient catalysts for solar energy conversion.<sup>141–143</sup> Recently, it has been revealed that plasmonic semiconductors, albeit at their incipient research stage, displayed superior activity in photocatalysis or photovoltaics as compared to their non-plasmonic counterparts.<sup>67,144</sup> The presence of cation or oxygen vacancies brings appreciable free carriers in non-stoichiometric semiconductors, ensuring them to harvest the sunlight in a broad range.

The first example for plasmon-enhanced photocatalytic reactions using non-metal semiconductors under visible light was illustrated on the  $\text{MoO}_{3-x}$  nanosheets.<sup>67</sup>  $\text{MoO}_{3-x}$  nanosheets, with the size ranging from 200 nm to 1  $\mu\text{m}$  (Fig. 16a), were prepared by oxidizing metal Mo powder with  $\text{H}_2\text{O}_2$  in ethanol solution and the subsequent solvothermal treatment. In contrast with commercial  $\text{MoO}_3$  that merely responds to UV light, strong visible light absorption was observed in the prepared  $\text{MoO}_{3-x}$  nanosheets with LSPR peak around 680 nm (Fig. 16b). X-ray photoelectron spectroscopy (XPS) measurement confirmed the presence of oxygen vacancies, with large amount of  $\text{Mo}^{5+}$  in the  $\text{MoO}_{3-x}$ . It was found that plasmonic  $\text{MoO}_{3-x}$  could be used as highly efficient catalyst to dehydrogenate  $\text{NH}_3\text{BH}_3$ . The plasmonic  $\text{MoO}_{3-x}$  outperformed the non-plasmonic commercial  $\text{MoO}_3$  both in dark condition and under visible light illumination. It was noted that compared to dark condition, visible light could dramatically enhance the catalytic activity by a factor of 4 on the plasmonic  $\text{MoO}_{3-x}$  (Fig. 16c). Through contrast experiments, plasmonic effect accounted the predominant contribution (*ca.* 77%) to the catalytic enhancement (Fig. 16d).

To induce metallic behavior in semiconductors, highly doping by defect chemistry is a precondition. The presence of defects enables plasmonic semiconductors, especially self-doped semiconductors, to have more active sites for reaction, and could be promising for heterogeneous catalysis. The as-prepared plasmonic  $\text{MoO}_{3-x}$  nanosheets showed highly efficient activity in dehydrogenation of  $\text{NH}_3\text{BH}_3$  with visible light, even exceeding plasmonic noble metals of Ag/SBA-15.<sup>67</sup> This work demonstrates a facile access to semiconductor nanostructures with strong LSPR absorption in the visible light range, being comparable to noble metals. In addition, the plasmonic semiconductors can also be employed for efficient visible light-driven photocatalysis, and it offers the potential utilization of the earth-abundant elements instead of the precious noble metals to a certain extent.

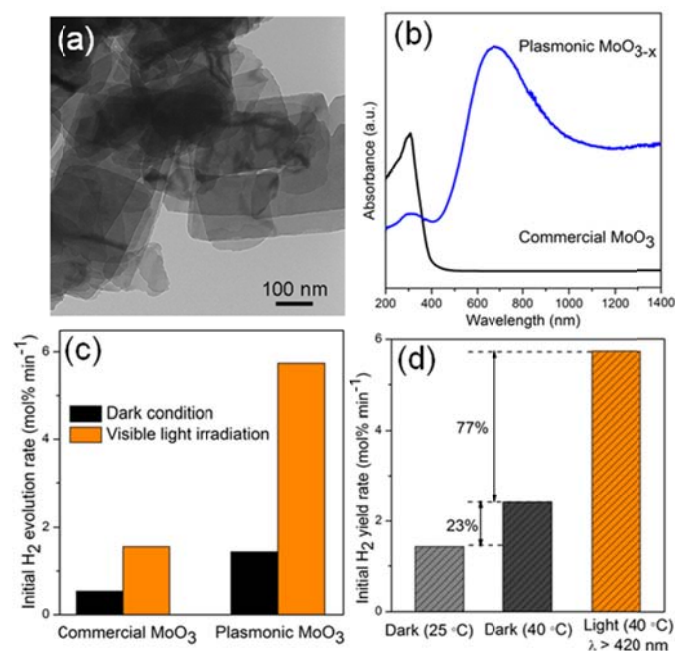


Fig. 16 (a) TEM image of  $\text{MoO}_{3-x}$  nanosheets, (b) UV/Vis-NIR optical absorption of  $\text{MoO}_{3-x}$  and commercial  $\text{MoO}_3$ , (c) comparison of initial  $\text{H}_2$  yield rate over  $\text{MoO}_{3-x}$  and commercial  $\text{MoO}_3$  samples with and without light irradiation, and (d) thermal effect on the catalytic performance of  $\text{MoO}_{3-x}$  in dark conditions and under visible light irradiation. Adapted with permission from ref. 67. Copyright 2014 Wiley-VCH.

## 4. Summary and outlook

Plasmonic metallic nanostructures, including noble metals and highly-doped semiconductors, represent a class of promising materials that integrate the light-responsive and catalytic-active properties. Through an excitation of LSPR, the hot electrons generated on the surface of metallic NPs are able to migrate to the contiguous semiconductors, or directly activate the adsorbed molecules and drive their catalytic reactions. The plasmon-mediated photocatalysis, with the assistance of near-field enhancement and electron density at the Fermi level,<sup>8</sup> usually surpasses conventional semiconductor photocatalysis. The introduction of LSPR into photocatalysis has opened up

new avenues for efficient conversion of the abundant sunlight into chemical energy.

The photocatalytic reactions involve the participation of oxidizing and reducing agents in the following redox procedures; hence interfacial charge transfer is a key to understand the underlying mechanism. Despite the fact that direct chemical reactions occur on the adsorbed molecules, vectorial electron transfer between metal NPs and the supports is required to obtain higher efficiency. On one hand, prior to recombination, plasmon-induced energetic electrons are able to cross the Schottky barrier between noble metals and wide band semiconductors, leading to interfacial charge separation. On the other hand, the presence of strong metal-support interactions (SMSI) enables the inherent electronic and chemical stability of surface noble metals,<sup>145,146</sup> and thus reducible oxide semiconductors (*e.g.*, CeO<sub>2</sub>, TiO<sub>2</sub>) usually outperform the non-reducible ones (*e.g.*, Al<sub>2</sub>O<sub>3</sub>, ZrO<sub>2</sub>) to support the plasmonic photocatalysis of metal NPs. Therefore, for specific reactions with favorable electron-withdrawing or donating effect, it is of crucial importance to choose appropriate oxide support materials.

As the most investigated plasmonic photocatalysts, Au and Ag nanostructures have been paid much attention. Nevertheless, the high cost and earth-rarity restrict their large-scale practical applications. It seems more appealing to use earth-abundant plasmonic elements/oxides such as Cu, Al and MoO<sub>3-x</sub> with comparable plasmonic absorption to Au and Ag in the visible light region. To this end, the control of their surface oxidation states and guarantee of their chemical stability should be well addressed. The presence of light irradiation<sup>31</sup> or hybridization with electron-rich graphene<sup>130</sup> has turned out to be possible routes to protect and maintain the stabilities of the instable plasmonic metal nanostructures. Other strategies, for example, photoelectrocatalysis with the aid of voltage bias, could be further developed to enhance the plasmonic-mediated photocatalysis as well as the chemical stability of metallic nanostructures.

In single-active plasmonic photocatalysis, metallic NPs function as both the photo- and catalytic-active sites, and they have shown high potentials in selective organic transformation with mild oxidation ability. In addition to enhancing the catalysis of metallic NPs themselves, the surface plasmons do have the ability to boost the catalytic activities of adjacent semiconductors, molecular complexes as well as metal NPs. Among these, metal/semiconductor hybrids account for the majority and have been applied dominantly to improve the photocatalytic performance of semiconductors in water splitting and toxic pollutants removal. Recently, electron transfer from the plasmonic metals to the other catalytic ones could also improve the photocatalytic activity of the latter in chemical synthesis, such as Pd-catalyzed Suzuki-coupling reactions<sup>147–149</sup> and Ru-catalyzed ammonia synthesis.<sup>150</sup>

Albeit with the arresting progress, plasmon-directed photocatalysis is still in its infancy. A great many issues such as the interfacial structure, band alignment and contacting architectures between plasmonic metals and support materials

should be clarified for preferential charge transfer. The plasmonic property of metallic nanostructures is strongly dependent on their metal species, sizes, shapes and supporting materials, which in turn offer the guidelines and protocols to allow one to harvest the broad absorption across the whole solar spectrum by harnessing the rationally devised nanostructures. With the on-going in-depth investigations, it is envisaged that this burgeoning field will bring greater achievements in exploiting highly efficient and robust plasmonic photocatalysts working under visible light.

## Acknowledgements

Part of this work was performed under a management of 'Elements Strategy Initiative for Catalysts & Batteries (ESICB)' supported by Ministry of Education Culture, Sports, Science, and Technology (MEXT) program, Japan. H.C. would like to thank Japan Society for the Promotion of Science (JSPS) for the fellowship.

## Notes and references

<sup>a</sup> Division of Materials and Manufacturing Science, Graduate School of Engineering, Osaka University, 2-1 Yamada-oka, Suita, Osaka 565-0871, Japan. E-mail: yamashita@mat.eng.osaka-u.ac.jp

<sup>b</sup> Unit of Elements Strategy Initiative for Catalysts & Batteries, Kyoto University, Katsura, Kyoto 615-8520, Japan

- 1 N. S. Lewis and D. G. Nocera, *Proc. Natl. Acad. Sci.*, 2006, **103**, 15729–15735.
- 2 X. Lang, X. Chen and J. Zhao, *Chem. Soc. Rev.*, 2014, **43**, 473–486.
- 3 A. Fujishima and K. Honda, *Nature*, 1972, **238**, 37–38.
- 4 M. R. Hoffmann, S. T. Martin, W. Choi and D. W. Bahnemann, *Chem. Rev.*, 1995, **95**, 69–96.
- 5 A. Kudo and Y. Miseki, *Chem. Soc. Rev.*, 2009, **38**, 253–278.
- 6 X. Chen, S. Shen, L. Guo and S. S. Mao, *Chem. Rev.*, 2010, **110**, 6503–6570.
- 7 Y. Shiraiishi and T. Hirai, *J. Photochem. Photobiol., C*, 2008, **9**, 157–170.
- 8 S. Linic, P. Christopher and D. B. Ingram, *Nat. Mater.*, 2011, **10**, 911–921.
- 9 K. Watanabe, D. Menzel, N. Nilius and H. J. Freund, *Chem. Rev.*, 2006, **106**, 4301–4320.
- 10 M. Rycenga, C. M. Cogley, J. Zeng, W. Li, C. H. Moran, Q. Zhang, D. Qin and Y. Xia, *Chem. Rev.*, 2011, **111**, 3669–3712.
- 11 H. Chen, L. Shao, Q. Li and J. Wang, *Chem. Soc. Rev.*, 2013, **42**, 2679–2724.
- 12 S. Nie and S. R. Emory, *Science*, 1997, **275**, 1102–1106.
- 13 E. M. van Schrojenstein Lantman, T. Deckert-Gaudig, A. J. G. Mank, V. Deckert and B. M. Weckhuysen, *Nat. Nanotechnol.*, 2012, **7**, 583–586.
- 14 S. Lal, N. K. Grady, J. Kundu, C. S. Levin, J. B. Lassiter and N. J. Halas, *Chem. Soc. Rev.*, 2008, **37**, 898–911.

- 15 M. E. Stewart, C. R. Anderton, L. B. Thompson, J. Maria, S. K. Gray, J. A. Rogers and R. G. Nuzzo, *Chem. Rev.*, 2008, **108**, 494–521.
- 16 D. K. Lim, K. S. Jeon, H. M. Kim, J. M. Nam and Y. D. Suh, *Nat. Mater.*, 2010, **9**, 60–67.
- 17 V. E. Ferry, L. A. Sweatlock, D. Pacifici and H. A. Atwater, *Nano Lett.*, 2008, **8**, 4391–4397.
- 18 P. K. Jain, X. Huang, I. H. El-Sayed and M. A. El-Sayed, *Plasmonics*, 2007, **2**, 107–118.
- 19 H. Tada, T. Mitsui, T. Kiyonaga, T. Akita and K. Tanaka, *Nat. Mater.*, 2006, **5**, 782–786.
- 20 K. Awazu, M. Fujimaki, C. Rockstuhl, J. Tominaga, H. Murakami, Y. Ohki, N. Yoshida and T. Watanabe, *J. Am. Chem. Soc.*, 2008, **130**, 1676–1680.
- 21 P. Wang, B. Huang, X. Qin, X. Zhang, Y. Dai, J. Wei and M. H. Whangbo, *Angew. Chem. Int. Ed.*, 2008, **47**, 7931–7933.
- 22 Z. Liu, W. Hou, P. Pavaskar, M. Aykol and S. B. Cronin, *Nano Lett.*, 2011, **11**, 1111–1116.
- 23 H. Cheng, B. Huang, P. Wang, Z. Wang, Z. Lou, J. Wang, X. Qin, X. Zhang and Y. Dai, *Chem. Commun.*, 2011, **47**, 7054–7056.
- 24 S. Mubeen, J. Lee, N. Singh, S. Krämer, G. D. Stucky and M. Moskovits, *Nat. Nanotechnol.*, 2013, **8**, 247–251.
- 25 A. Tanaka, K. Hashimoto and H. Kominami, *J. Am. Chem. Soc.*, 2014, **136**, 586–589.
- 26 Z. Bian, T. Tachikawa, P. Zhang, M. Fujitsuka and T. Majima, *J. Am. Chem. Soc.*, 2014, **136**, 458–465.
- 27 K. Mori, M. Kawashima, M. Che and H. Yamashita, *Angew. Chem. Int. Ed.*, 2010, **49**, 8598–8601.
- 28 X. Chen, H. Y. Zhu, J. C. Zhao, Z. F. Zheng and X. P. Gao, *Angew. Chem. Int. Ed.*, 2008, **47**, 5353–5356.
- 29 H. Zhu, X. Ke, X. Yang, S. Sarina and H. Liu, *Angew. Chem. Int. Ed.*, 2010, **49**, 9657–9661.
- 30 P. Christopher, H. Xin and S. Linic, *Nat. Chem.*, 2011, **3**, 467–472.
- 31 A. Marimuthu, J. Zhang and S. Linic, *Science*, 2013, **339**, 1590–1593.
- 32 S. C. Warren and E. Thimsen, *Energy Environ. Sci.*, 2012, **5**, 5133–5146.
- 33 X. Zhou, G. Liu, J. Yu and W. Fan, *J. Mater. Chem.*, 2012, **22**, 21337–21354.
- 34 P. Wang, B. Huang, Y. Dai and M. H. Whangbo, *Phys. Chem. Chem. Phys.*, 2012, **14**, 9813–9825.
- 35 W. Hou and S. B. Cronin, *Adv. Funct. Mater.*, 2013, **23**, 1612–1619.
- 36 M. Xiao, R. Jiang, F. Wang, C. Fang, J. Wang and J. C. Yu, *J. Mater. Chem. A*, 2013, **1**, 5790–5805.
- 37 R. Jiang, B. Li, C. Fang and J. Wang, *Adv. Mater.*, 2014, **26**, 5274–5309.
- 38 Z. Lou, Z. Wang, B. Huang and Y. Dai, *ChemCatChem*, 2014, **6**, 2456–2476.
- 39 Q. Xiao, E. Jaatinen and H. Zhu, *Chem. Asian J.*, 2014, **11**, 3046–3064.
- 40 M. J. Kale, T. Avanesian and P. Christopher, *ACS Catal.*, 2014, **4**, 116–128.
- 41 C. J. DeSantis, R. G. Weiner, A. Radmilovic, M. M. Bower and S. E. Skrabalak, *J. Phys. Chem. Lett.*, 2013, **4**, 3072–3082.
- 42 N. E. Motl, A. F. Smith, C. J. DeSantis and S. E. Skrabalak, *Chem. Soc. Rev.*, 2014, **43**, 3823–3834.
- 43 S. A. Maier, *Plasmonics: Fundamentals and Applications*, Springer, 2007.
- 44 M. A. Garcia, *J. Phys. D: Appl. Phys.*, 2011, **44**, 283001.
- 45 J. A. Creighton and D. G. Eadont, *J. Chem. Soc. Faraday Trans.*, 1991, **87**, 3881–3891.
- 46 C. Langhammer, M. Schwind, B. Kasemo and I. Zorić, *Nano Lett.*, 2008, **8**, 1461–1471.
- 47 N. J. M. Sanghamitra and S. Mazumdar, *Langmuir*, 2008, **24**, 3439–3445.
- 48 C. Langhammer, Z. Yuan, I. Zorić and B. Kasemo, *Nano Lett.*, 2006, **6**, 833–838.
- 49 X. Huang, S. Tang, X. Mu, Y. Dai, G. Chen, Z. Zhou, F. Ruan, Z. Yang and N. Zheng, *Nat. Nanotechnol.*, 2011, **6**, 28–32.
- 50 P. Mulvaney, *Langmuir*, 1996, **12**, 788–800.
- 51 K. L. Kelly, E. Coronado, L. L. Zhao and G. C. Schatz, *J. Phys. Chem. B*, 2003, **107**, 668–677.
- 52 X. Lu, M. Rycenga, S. E. Skrabalak, B. Wiley and Y. Xia, *Annu. Rev. Phys. Chem.*, 2009, **60**, 167–192.
- 53 H. Wang, F. Tam, N. K. Grady and N. J. Halas, *J. Phys. Chem. B*, 2005, **109**, 18218–18222.
- 54 K. Fuku, S. Takakura, T. Kamegawa, K. Mori and H. Yamashita, *Chem. Lett.*, 2012, **41**, 614–616.
- 55 M. Hu, J. Chen, Z. Y. Li, L. Au, G. V. Hartland, X. Li, M. Marqueze and Y. Xia, *Chem. Soc. Rev.*, 2006, **35**, 1084–1094.
- 56 P. Lignier, R. Bellabarba and R. P. Tooze, *Chem. Soc. Rev.*, 2012, **41**, 1708–1720.
- 57 C. Clavero, *Nat. Photonics*, 2014, **8**, 95–103.
- 58 M. A. Mahmoud, M. Chamanzar, A. Adibi and M. A. El-Sayed, *J. Am. Chem. Soc.*, 2012, **134**, 6434–6442.
- 59 M. Kanehara, H. Koike, T. Yoshinaga and T. Teranishi, *J. Am. Chem. Soc.*, 2009, **131**, 17736–17737.
- 60 J. M. Luther, P. K. Jain, T. Ewers and A. P. Alivisatos, *Nat. Mater.*, 2011, **10**, 361–366.
- 61 Y. X. Zhao, H. C. Pan, Y. B. Lou, X. F. Qiu, J. J. Zhu and C. Burda, *J. Am. Chem. Soc.*, 2009, **131**, 4253–4261.
- 62 S. W. Hsu, K. On and A. R. Tao, *J. Am. Chem. Soc.*, 2011, **133**, 19072–19075.
- 63 Y. Xie, A. Riedinger, M. Prato, A. Casu, A. Genovese, P. Guardia, S. Sottini, C. Sangregorio, K. Miszta, S. Ghosh, T. Pellegrino and L. Manna, *J. Am. Chem. Soc.*, 2013, **135**, 17630–17637.
- 64 K. Manthiram and A. P. Alivisatos, *J. Am. Chem. Soc.*, 2012, **134**, 3995–3998.
- 65 T. R. Gordon, M. Cargnello, T. Paik, F. Mangolini, R. T. Weber, P. Fornasiero and C. B. Murray, *J. Am. Chem. Soc.*, 2012, **134**, 6751–6761.
- 66 Q. Huang, S. Hu, J. Zhuang and X. Wang, *Chem. Eur. J.*, 2012, **18**, 15283–15287.
- 67 H. Cheng, T. Kamegawa, K. Mori and H. Yamashita, *Angew. Chem. Int. Ed.*, 2014, **53**, 2910–2914.
- 68 M. M. Y. A. Alsaif, K. Latham, M. R. Field, D. D. Yao, N. V. Medehkar, G. A. Beane, R. B. Kaner, S. P. Russo, J. Z. Ou and K. Kalantar-zadeh, *Adv. Mater.*, 2014, **26**, 3931–3937.
- 69 X. Liu and M. T. Swihart, *Chem. Soc. Rev.*, 2014, **43**, 3908–3920.
- 70 A. Comin and L. Manna, *Chem. Soc. Rev.*, 2014, **43**, 3957–3975.
- 71 X. Ma, Y. Dai, L. Yu and B. Huang, *Sci. Rep.*, 2014, **4**, 3986.
- 72 F. Le, D. W. Brandl, Y. A. Urzhumov, H. Wang, J. Kundu, N. J. Halas, J. Aizpurua and P. Nordlander, *ACS Nano*, 2008, **2**, 707–718.
- 73 H. Cheng, B. Huang and Y. Dai, *Nanoscale*, 2014, **6**, 2009–2026.

- 74 A. Furube, L. Du, K. Hara, R. Katoh and M. Tachiya, *J. Am. Chem. Soc.*, 2007, **129**, 14852–14853.
- 75 T. Fujita, P. Guan, K. McKenna, X. Lang, A. Hirata, L. Zhang, T. Tokunaga, S. Arai, Y. Yamamoto, N. Tanaka, Y. Ishikawa, N. Asao, Y. Yamamoto, J. Erlebacher and M. Chen, *Nat. Mater.*, 2012, **11**, 775–780.
- 76 G. L. Hallett-Tapley, M. J. Silvero, M. González-Béjar, M. Grenier, J. C. Netto-Ferreira and J. C. Scaiano, *J. Phys. Chem. C*, 2011, **115**, 10784–10790.
- 77 T. L. Wee, L. C. Schmidt and J. C. Scaiano, *J. Phys. Chem. C*, 2012, **116**, 24373–24379.
- 78 C. J. B. Alejo, C. Fasciani, M. Grenier, J. C. Netto-Ferreira and J. C. Scaiano, *Catal. Sci. Technol.*, 2011, **1**, 1506–1511.
- 79 J. Robertson, *J. Vac. Sci. Technol. B*, 2000, **18**, 1785–1791.
- 80 M. W. Knight, H. Sobhani, P. Nordlander and N. J. Halas, *Science*, 2011, **332**, 702–704.
- 81 H. Zhu, X. Chen, Z. Zheng, X. Ke, E. Jaatinen, J. Zhao, C. Guo, T. Xie and D. Wang, *Chem. Commun.*, 2009, 7524–7526.
- 82 L. Gómez, J. L. Hueso, M. C. Ortega-Liébana, J. Santamaría and S. B. Cronin, *Catal. Commun.*, 2014, **56**, 115–118.
- 83 L. Gomez, V. Sebastian, M. Arruebo, J. Santamaria and S. B. Cronin, *Phys. Chem. Chem. Phys.*, 2014, **16**, 15111–15116.
- 84 X. Ke, X. Zhang, J. Zhao, S. Sarina, J. Barry and H. Zhu, *Green Chem.*, 2013, **15**, 236–244.
- 85 C. D. Pina, E. Falletta and M. Rossi, *Chem. Soc. Rev.*, 2012, **41**, 350–369.
- 86 X. Zhang, X. Ke and H. Zhu, *Chem. Eur. J.*, 2012, **18**, 8048–8056.
- 87 G. L. Hallett-Tapley, M. J. Silvero, C. J. Bueno-Alejo, M. González-Béjar, C. D. McTiernan, M. Grenier, J. C. Netto-Ferreira and J. C. Scaiano, *J. Phys. Chem. C*, 2013, **117**, 12279–12288.
- 88 A. Pineda, L. Gomez, A. M. Balu, V. Sebastian, M. Ojeda, M. Arruebo, A. A. Romero, J. Santamaria and R. Luque, *Green Chem.*, 2013, **15**, 2043–2049.
- 89 Y. Zhang, Q. Xiao, Y. Bao, Y. Zhang, S. Bottle, S. Sarina, B. Zhaorigetu and H. Zhu, *J. Phys. Chem. C*, 2014, **118**, 19062–19069.
- 90 P. Christopher, H. Xin, A. Marimuthu and S. Linic, *Nat. Mater.*, 2012, **11**, 1044–1050.
- 91 X. Chen, Z. Zheng, X. Ke, E. Jaatinen, T. Xie, D. Wang, C. Guo, J. Zhao and H. Zhu, *Green Chem.*, 2010, **12**, 414–419.
- 92 K. H. Chen, Y. C. Pu, K. D. Chang, Y. F. Liang, C. M. Liu, J. W. Yeh, H. C. Shih and Y. J. Hsu, *J. Phys. Chem. C*, 2012, **116**, 19039–19045.
- 93 M. Yadav and Q. Xu, *Energy Environ. Sci.*, 2012, **5**, 9698–9725.
- 94 K. Fuku, R. Hayashi, S. Takakura, T. Kamegawa, K. Mori and H. Yamashita, *Angew. Chem. Int. Ed.*, 2013, **52**, 7446–7450.
- 95 C. Ho, J. C. Yu, T. Kwong, A. C. Mak and S. Lai, *Chem. Mater.*, 2005, **17**, 4514–4522.
- 96 Y. Xu and M. A. A. Schoonen, *Am. Mineral.*, 2000, **85**, 543–556.
- 97 S. Mukherjee, L. Zhou, A. M. Goodman, N. Large, C. Ayala-Orozco, Y. Zhang, P. Nordlander and N. J. Halas, *J. Am. Chem. Soc.*, 2014, **136**, 64–67.
- 98 J. Sá, G. Tagliabue, P. Friedli, J. Szlachetko, M. H. Rittmann-Frank, F. G. Santomauro, C. J. Milne and H. Sigg, *Energy Environ. Sci.*, 2013, **6**, 3584–3588.
- 99 X. Ma, Y. Dai, L. Yu and B. Huang, *ACS Appl. Mater. Interfaces*, 2014, **6**, 12388–12394.
- 100 X. Ma, Y. Dai, M. Guo, Y. Zhu and B. Huang, *Phys. Chem. Chem. Phys.*, 2013, **15**, 8722–8731.
- 101 E. Kowalska, O. O. P. Mahaney, R. Abea and B. Ohtani, *Phys. Chem. Chem. Phys.*, 2010, **12**, 2344–2355.
- 102 A. Tanaka, A. Ogino, M. Iwaki, K. Hashimoto, A. Ohnuma, F. Amano, B. Ohtani and H. Kominami, *Langmuir*, 2012, **28**, 13105–13111.
- 103 A. Tanaka, Y. Nishino, S. Sakaguchi, T. Yoshikawa, K. Imamura, K. Hashimoto and H. Kominami, *Chem. Commun.*, 2013, **49**, 2551–2553.
- 104 A. Tanaka, K. Hashimoto, B. Ohtani and H. Kominami, *Chem. Commun.*, 2013, **49**, 3419–3421.
- 105 D. Tsukamoto, Y. Shiraishi, Y. Sugano, S. Ichikawa, S. Tanaka and T. Hirai, *J. Am. Chem. Soc.*, 2012, **134**, 6309–6315.
- 106 S. Naya, A. Inoue and H. Tada, *J. Am. Chem. Soc.*, 2010, **132**, 6292–6293.
- 107 A. Tanaka, K. Hashimoto and H. Kominami, *Chem. Commun.*, 2011, **47**, 10446–10448.
- 108 A. Tanaka, K. Hashimoto and H. Kominami, *J. Am. Chem. Soc.*, 2012, **134**, 14526–14533.
- 109 A. Maldotti, A. Molinari, R. Juárez and H. Garcia, *Chem. Sci.*, 2011, **2**, 1831–1834.
- 110 S. Naya, M. Teranishi, T. Isobeb and H. Tada, *Chem. Commun.*, 2010, **46**, 815–817.
- 111 Y. Ide, M. Matsuoka and M. Ogawa, *J. Am. Chem. Soc.*, 2010, **132**, 16762–16764.
- 112 Y. Ide, N. Nakamura, H. Hattori, R. Ogino, M. Ogawa, M. Sadakane and T. Sano, *Chem. Commun.*, 2011, **47**, 11531–11533.
- 113 Z. Zheng, B. Huang, X. Qin, X. Zhang, Y. Dai and M. H. Whangbo, *J. Mater. Chem.*, 2011, **21**, 9079–9087.
- 114 S. Naya, K. Kimura and H. Tada, *ACS Catal.*, 2013, **3**, 10–13.
- 115 X. Ke, S. Sarina, J. Zhao, X. Zhang, J. Chang and H. Zhu, *Chem. Commun.*, 2012, **48**, 3509–3511.
- 116 S. Naya, T. Niwa, T. Kume and H. Tada, *Angew. Chem. Int. Ed.*, 2014, **53**, 7305–7309.
- 117 J. Zhao, Z. Zheng, S. Bottle, A. Chou, S. Sarina and H. Zhu, *Chem. Commun.*, 2013, **49**, 2676–2678.
- 118 X. Ma, Y. Dai, L. Yu, Z. Lou, B. Huang and M. H. Whangbo, *J. Phys. Chem. C*, 2014, **118**, 12133–12140.
- 119 M. González-Béjar, K. Peters, G. L. Hallett-Tapley, M. Grenier and J. C. Scaiano, *Chem. Commun.*, 2013, **49**, 1732–1734.
- 120 J. Liu, R. Si, H. Zheng, Q. Geng, W. Dai, X. Chen and X. Fu, *Catal. Commun.*, 2012, **26**, 136–139.
- 121 K. Yang, J. Liu, R. Si, X. Chen, W. Dai and X. Fu, *J. Catal.*, 2014, **317**, 229–239.
- 122 M. M. Titirici, R. J. White, N. Brun, V. L. Budarin, D. S. Su, F. del Monte, J. H. Clark and M. J. MacLachlan, *Chem. Soc. Rev.*, 2015, **44**, 250–290.
- 123 J. Li, C. Y. Liu and Z. Xie, *Mater. Res. Bull.*, 2011, **46**, 743–747.
- 124 T. Wu, S. Liu, Y. Luo, W. Lu, L. Wang and X. Sun, *Nanoscale*, 2011, **3**, 2142–2144.
- 125 V. G. Kravets, R. Jalil, Y. J. Kim, D. Ansell, D. E. Aznabayeva, B. Thackray, L. Britnell, B. D. Belle, F. Withers, I. P. Radko, Z. Han, S. I. Bozhevolnyi, K. S. Novoselov, A. K. Geim and A. N. Grigorenko, *Sci. Rep.*, 2014, **4**, 5517.

- 126 S. Sun, W. Wang, L. Zhang, M. Shang and L. Wang, *Catal. Commun.*, 2009, **11**, 290–293.
- 127 A. K. Geim and K. S. Novoselov, *Nat. Mater.*, 2007, **6**, 183–191.
- 128 Z. Xiong, L. L. Zhang, J. Ma and X. S. Zhao, *Chem. Commun.*, 2010, **46**, 6099–6101.
- 129 Y. Haldorai, B. K. Kim, Y. L. Jo and J. J. Shim, *Mater. Chem. Phys.*, 2014, **143**, 1452–1461.
- 130 X. Guo, C. Hao, G. Jin, H. Y. Zhu and X. Y. Guo, *Angew. Chem. Int. Ed.*, 2014, **53**, 1973–1977.
- 131 M. Sun and H. Xu, *Small*, 2012, **8**, 2777–2786.
- 132 B. Dong, Y. Fang, X. Chen, H. Xu and M. Sun, *Langmuir*, 2011, **27**, 10677–10682.
- 133 J. Ye, J. A. Hutchison, H. Uji-i, J. Hofkens, L. Lagae, G. Maes, G. Borghs and P. V. Dorpe, *Nanoscale*, 2012, **4**, 1606–1611.
- 134 Z. G. Dai, X. H. Xiao, Y. P. Zhang, F. Ren, W. Wu, S. F. Zhang, J. Zhou, F. Mei and C. Z. Jiang, *Nanotechnology*, 2012, **23**, 335701.
- 135 L. Kang, P. Xu, B. Zhang, H. Tsai, X. Han and H. L. Wang, *Chem. Commun.*, 2013, **49**, 3389–3391.
- 136 X. Zhang, P. Wang, Z. Zhang, Y. Fang and M. Sun, *Sci. Rep.*, 2014, **4**, 5407.
- 137 Y. F. Huang, M. Zhang, L. B. Zhao, J. M. Feng, D. Y. Wu, B. Ren and Z. Q. Tian, *Angew. Chem. Int. Ed.*, 2014, **53**, 2353–2357.
- 138 Y. Zong, Q. Guo, M. Xu, Y. Yuan, R. Gu and J. Yao, *RSC Adv.*, 2014, **4**, 31810–31816.
- 139 L. Kubus, H. Erdogan, S. S. Cetin, E. Biskin and G. Demirel, *ChemCatChem*, 2013, **5**, 2973–2977.
- 140 J. H. Kim, K. M. Twaddle, J. Hu and H. Byun, *ACS Appl. Mater. Interfaces*, 2014, **6**, 11514–11522.
- 141 J. Papp, S. Soled, K. Dwight and A. Wold, *Chem. Mater.*, 1994, **6**, 496–500.
- 142 M. Vasilopoulou, A. M. Douvas, D. G. Georgiadou, L. C. Palilis, S. Kennou, L. Sygellou, A. Soutlati, I. Kostis, G. Papadimitropoulos, D. Davazoglou and P. Argitis, *J. Am. Chem. Soc.*, 2012, **134**, 16178–16187.
- 143 H. J. Lewerenz, H. Goslowsky, K. D. Husemann and S. Fiechter, *Nature*, 1986, **321**, 687–688.
- 144 J. S. Niezgodna, E. Yap, J. D. Keene, J. R. McBride and S. J. Rosenthal, *Nano Lett.*, 2014, **14**, 3262–3269.
- 145 S. J. Tauster, S. C. Fung and R. L. Garten, *J. Am. Chem. Soc.*, 1978, **100**, 170–175.
- 146 Q. Fu, F. Yang and X. Bao, *Acc. Chem. Res.*, 2013, **46**, 1692–1701.
- 147 F. Wang, C. Li, H. Chen, R. Jiang, L. D. Sun, Q. Li, J. Wang, J. C. Yu and C. H. Yan, *J. Am. Chem. Soc.*, 2013, **135**, 5588–5601.
- 148 S. Sarina, H. Zhu, E. Jaatinen, Q. Xiao, H. Liu, J. Jia, C. Chen and J. Zhao, *J. Am. Chem. Soc.*, 2013, **135**, 5793–5801.
- 149 X. Huang, Y. Li, Y. Chen, H. Zhou, X. Duan and Y. Huang, *Angew. Chem. Int. Ed.*, 2013, **52**, 6063–6067.
- 150 T. Oshikiri, K. Ueno and H. Misawa, *Angew. Chem. Int. Ed.*, 2014, **53**, 9802–9805.